The Canadian Mineralogist
Vol. 48, pp. 351-359 (2010)
DOI: 10.3749/canmin.48.2.351

IRRADIATION DAMAGE IN MONAZITE-(Ce): AN EXAMPLE TO ESTABLISH THE LIMITS OF RAMAN CONFOCALITY AND DEPTH RESOLUTION

LUTZ NASDALA§

Institut für Mineralogie und Kristallographie, Universität Wien, Althanstr. 14, A–1090 Wien, Austria

RAINER GRÖTZSCHEL AND SYLVIO PROBST

Institut für Ionenstrahlphysik und Materialforschung, Forschungszentrum Dresden-Rossendorf e.V., P.O. Box 510119, D–01314 Dresden, Germany

BERND BLEISTEINER

Horiba Jobin Yvon GmbH, Neuhofstr. 9, D–64625 Bensheim, Germany

ABSTRACT

Crystals of synthetic monazite-(Ce), and foils of the same material 1 μm thick, were irradiated with 1, 3.5, and 7 MeV Au ions, with total fluences in the range 0.6–51 × 10^{13} ions/cm^2. The triple irradiation resulted in surficial structural damage extending up to ~1.5 μm into the samples. The irradiation damage generated was studied using Raman microspectroscopy. At low doses of irradiation, internal stretching bands of the PO_4 groups show significant broadening (reflecting a decrease in short-range order and increase in strain in the remnant crystalline volume-fraction of the radiation-damaged solid), which is accompanied by notable losses in intensity and shifts of bands toward lower wavenumbers. At the highest dose of irradiation, the material has become amorphous, and the "crystalline" PO_4 Raman modes disappeared. These observations, however, were only made in the case of the thin lamella prepared using a focused ion-beam system. The Raman spectra of the analogously irradiated, unprepared crystals are dominated by bands of apparently undamaged, crystalline $CePO_4$. We assign the latter to the host crystal underneath the surficial, damaged region, which contributes strongly to the spectrum obtained because of the insufficient depth-resolution of the confocal spectrometer. Limits in confocality, and the related potential misinterpretation of spectroscopic results, must be considered.

Keywords: monazite-(Ce), radiation damage, Raman spectroscopy, confocality, focused ion beam.

SOMMAIRE

Nous avons irradié des cristaux de monazite-(Ce) synthétique, et des feuilles ultraminces (1 μm d'épaisseur) préparées à partir du même matériau, avec des ions de Au dans un faisceau de 1, 3.5, et 7 MeV, avec des fluences totales dans l'intervalle 0.6–51 × 10^{13} ions/cm^2. La triple irradiation a endommagé la surface des échantillons structuralement, jusqu'à une profondeur d'environ ~1.5 μm. Nous avons étudié le dommage ainsi généré au moyen de la microspectroscopie de Raman. A faibles taux d'irradiation, les modes d'étirement internes des groupes PO_4 causent un élargissement important des bandes (témoignant d'une diminution du degré d'ordre à courte échelle et une augmentation des déformations dans la fraction du volume du solide ayant encore une cristallinité) qui est accompagné par des pertes importantes en intensité et un déplacement des bandes vers les nombres d'onde plus faibles. Aux taux d'irradiation les plus intenses, le matériau passe à l'état amorphe, et les modes Raman "cristallins" de PO_4 ont disparus. Ces observations n'ont été faites que sur les feuilles ultraminces traitées avec un faisceau d'ions focalisé, toutefois. Les spectres Raman des cristaux non préparés ayant subi une irradiation analogue montrent une prédominance des bandes attribuables au $CePO_4$ sain, non endommagé. Ces bandes proviendraient du cristal hôte en dessous de la région de surface endommagée, qui contribue largement au spectre obtenu à cause de la résolution nettement insuffisante de la profondeur par le spectromètre confocal. On doit prendre en considération les limitations en matière de confocalisation et les fausses interprétations des résultats spectroscopiques qui pourraient en résulter.

(Traduit par la Rédaction)

Mots-clés: monazite-(Ce), dommage par irradiation, spectroscopie de Raman, confocalisation, faisceau d'ions focalisé.

§ *E-mail address*: lutz.nasdala@univie.ac.at

Introduction

Raman spectroscopy has proven to be an excellent means for analyzing non-destructively the chemical and structural properties of geological samples, with a spatial resolution on the micrometer scale. Accordingly, the number of authors using this technique and publishing in peer-reviewed Earth sciences journals has increased tremendously in the last decade, with applications covering virtually all subdisciplines. Even though Raman spectroscopy is commonly used merely as a fingerprinting technique, to identify minute quantities of phases, this technique offers a variety of exciting analytical possibilities. These include, among others, determination of the orientation of crystals or molecular groups, evaluation of strain or "fossilized pressures", determination of temperature, and estimates of the degree of short-range order. The latter is increasingly used in the investigation of radiation-induced structural damage of minerals (*e.g.*, Nasdala *et al.* 1995, 2003, 2007, Seydoux-Guillaume *et al.* 2002, Tomašic *et al.* 2004, Delattre *et al.* 2007, Anderson *et al.* 2008, Dias *et al.* 2009, Gieré *et al.* 2009). These studies aim at a better understanding of the changed physical properties and chemical resistance of radiation-damaged solids, when compared to their undamaged analogs, which is of enormous interest for the Earth sciences (*e.g.*, reliable interpretation of radiometric age data obtained from radiation-damaged accessories) and the materials sciences (*e.g.*, performance assessment of potential host ceramics for the long-term immobilization of nuclear waste; Ewing & Wang 2002).

One major advantage of Raman spectroscopy is its excellent spatial resolution. In a significant fraction of recent research contributions in the Earth sciences, however, the actual lateral and depth resolutions of confocal Raman systems are estimated incorrectly. Failure to accurately determine the true spatial resolution may in some cases lead to erroneous interpretations of analytical results. Zhang *et al.* (2008), for example, used conventional confocal Raman spectroscopy to analyze an only ~0.1 μm thick layer at the surface of a zircon crystal that was amorphized by irradiation with 280 keV Pb ions (fluence 10^{15} ions/cm^2). As the layer thickness is more than one order of magnitude smaller than the depth resolution of the analytical system used (which was presumably on the order of several μm), the "crystalline" Raman spectra of Zhang *et al.* (2008) cannot be assigned solely to the ~0.1 μm thick irradiation-damaged zone, but rather to an integrated volume of sample consisting of the amorphous region and the underlying host zircon (*cf.* also Nasdala 2009).

Insufficient consideration of the actual depth-resolution of confocal Raman analyses has, in our opinion, also adversely affected the interpretations in a recent study by Picot *et al.* (2008). These authors irradiated crystals of synthetic monazite-(La) ($LaPO_4$ and $La_{0.73}Ce_{0.27}PO_4$) with 1–7 MeV Au ions (0.96–230 × 10^{13} ions/cm^2) and 1.7 MeV He ions (fluences 1.09–54.3 × 10^{15} ions/cm^2). Picot *et al.* (2008) reported that the He irradiation had insignificantly affected the monazite crystal, whereas the Au irradiation resulted in major structural changes in surficial irradiation-damaged zones ≤1.5 μm thick. In spite of the heavy structural damage, up to amorphization at elevated doses of irradiation observed in the transmission electron microscope (TEM), "crystalline" Raman spectra with narrow bands were obtained. This observation led Picot *et al.* (2008) to the conclusion that phosphate tetrahedra must be remarkably stable, irradiation-resistant units. In contrast, we question the ability of a confocal Raman spectrometer system to accurately analyze a transparent, heavily damaged or amorphous layer ≤1.5 μm thick atop a transparent crystal without analyzing both materials. Rather, we assign the narrow Raman bands observed by Picot *et al.* (2008) to the co-analyzed, underlying bulk sample substrate, resulting in an integrated signal of the two materials.

To verify our alternative interpretation, and in particular to demonstrate the limits in confocality and possible consequences of their underestimation, we undertook a Raman study of Au-irradiated monazite-(Ce). We included both unprepared crystals and thin lamellae, and attempted to underline the necessity of appropriate preparation of the samples if phenomena are to be studied whose spatial extension is close to, or even below, the spatial resolution of the analytical system used.

Background Information

In the case of transparent samples, high spatial resolution of Raman spectroscopic analyses cannot be achieved simply by focusing the incident laser beam to a small diameter at a spot. Behind the focal plane, the light diverges and penetrates into the sample, and the lateral extension of the sample volume analyzed is hence much larger than the diameter of the focal-spot area (Wilson 1989, *cf.* also discussion in Nasdala *et al.* 2004). This problem can be reduced significantly by a confocal arrangement of the spectrometer's optical pathway. It should be emphasized again that the above problem is relevant particularly for transparent samples, whereas it is less significant if extremely thin or opaque materials are to be analyzed (Everall 2008). A much improved confocality, and hence better spatial resolution, can be achieved by placing a narrow aperture ("confocal hole") at a back-focal image plane (Tabaksblat *et al.* 1992), applying (software-controlled) pixel masking of the charge-coupled device (CCD) detector (Williams *et al.* 1994, Keen *et al.* 2002), or a combination of both methods.

Note that there exist two different definitions of what the term "spatial resolution" (being determined by both the lateral and the depth resolution) of a spectrometer

system describes. For single-point analyses, the spatial resolution is described commonly by the (maximum) size of the volume of sample analyzed. Second, it is possible to define spatial resolution by the minimum distance between two objects that can just be resolved (the so-called Rayleigh criterion, which is mostly used to define the spatial resolution of images or maps). For the latter definition, a significant but still incomplete suppression of signal originating outside the analyzed volume of sample is sufficient; this is why application of the second criterion above results in notably smaller estimates of the spatial resolution. Applying that second criterion, the maximal depth-resolution of a confocal Raman spectrometer can be estimated as $\sim 4\lambda/(NA)^2$ (Everall 2000, Baldwin & Batchelder 2001, and references therein). This approach, however, may easily underestimate the volume of sample that contributes potentially to the spectroscopic signal obtained (Everall 2008, 2009). In view of the generally better lateral resolution of confocal Raman spectrometers, compared to the in depth resolution, the effective spatial resolution of conventional Raman analyses of thin layers may be improved by applying lateral line-scanning of a cross-section prepared perpendicular to the surface layer investigated (Everall 2000) or the application of oil immersion instead of regular objectives. Analyses with a spatial resolution well beyond the diffraction limit may be made using surface-enhanced (SERS) or tip-enhanced Raman spectroscopy (TERS; *cf*. Hayazawa *et al*. 2007).

The above simple equation provides only a general estimate of the maximum performance of a spectrometer system with perfect alignment and infinitely small confocal aperture; it does not consider any effects of optical boundaries, such as refraction at the sample surface (Everall 2000, Bruneel *et al*. 2002). The real (*i.e*., experimentally confirmed) depth resolution is in general notably higher than the theoretically predicted value. Focus quality and shape of the laser beam will be distorted, and hence the depth resolution will be furthermore lowered as soon as the laser beam is focused deeper into a sample (as discussed in detail by Everall 2000, Baldwin & Batchelder 2001, Everall *et al*. 2007, Tfayli *et al*. 2008, Everall 2009). The latter is applicable, for instance, in the case of *in situ* analyses of inclusions or *z*-scans.

Materials and Methods

Samples investigated in this study are synthetic, pure (*i.e*., undoped) $CePO_4$ crystals. Crystals were grown using the lithium molybdate flux technique described by Hanchar *et al*. (2001). The euhedral, prismatic crystals are colorless and transparent and reach up to 5 mm in length.

To avoid any uncontrolled contribution of the unirradiated bulk crystal on the Raman spectra, it was necessary to use samples whose thicknesses are smaller than the depth of the irradiation damage. Five lamellae (rectangular shapes with average sizes of *ca*. 20 × 12 μm^2) were prepared using a Zeiss NVision 40 focused ion beam (FIB) system; the procedure is visualized in a number of secondary electron (SE) images in Figure 1. For details of the FIB preparation, see Wirth (2004). All lamellae were cut out from the same prism face of the same $CePO_4$ single crystal. After the final ion-beam polish, the lamellae were plane-parallel and had thicknesses of 0.9–1.1 μm (Fig. 1D). The lamellae were attached to separate metal sample holders by Pt ion deposition at their corners or edges. In case of the two irradiations with the lowest and highest ion-dose, an unprepared crystal was fixed at the same sample holder, with one (*i.e*., the top) prism face being oriented parallel to the main lamella face.

Four triple irradiations with Au ions were done in the standard implantation chamber of the 3 MV tandetron accelerator of the Forschungszentrum Dresden-Rossendorf (the fifth lamella was left unirradiated). The irradiation was done at room temperature, with the sample chamber being evacuated to $\sim 3 \times 10^{-7}$ mbar. By analogy with the experiments of Picot *et al*. (2008), samples were irradiated with equal doses of 1 MeV Au^+, 3.5 MeV Au^{2+}, and 7 MeV Au^{3+} ions. The fluences per ion energy were 0.2, 0.6, 1.8, and 17 × 10^{13} ions/cm^2, *i.e*., the total fluences for the four triple irradiations ranged from 0.6×10^{13} to 5.1×10^{14} ions/cm^2. To minimize potential ion channeling (*e.g*., Raineri *et al*. 1991), the ion beam was always directed with an angle of *ca*. 7° to the normal of the main lamella face and, where applicable, the top prism face of the neighboring unprepared crystal, respectively. The Au beam-scanning area was in each case larger than 40 × 40 mm^2 to keep the current density below 50 nA/cm^2 and to ensure simultaneous irradiation of lamella and unprepared crystal with equal fluence.

Raman analyses in quasi-back-scatter geometry were performed using a Horiba Jobin Yvon LabRam–HR spectrometer (focal length 800 mm). This dispersive system was equipped with Rayleigh rejection filter, Olympus BX41 optical microscope, a diffraction grating with 1800 grooves per millimeter, and Peltier-cooled, Si-based CCD detector. Spectra were excited with the 632.8 nm excitation of a He–Ne laser (~3 mW measured behind the microscope objective). An Olympus 100× objective (NA = 0.9) was used, and the system was operated in the confocal mode (confocal pinhole set to 100 μm). Wavenumber calibration was done using neon lamp emissions and the Rayleigh line, and the wavenumber accuracy was better than 0.5 cm^{-1}. The entrance slit was set to 100 μm, corresponding to a spectral resolution of 0.8 cm^{-1} at 632.8 nm excitation. Accumulation times were varied between 2 × 15 s for the unirradiated crystal and up to 2 × 600 s for irradiated lamellae. Band fitting was done after subtracting a

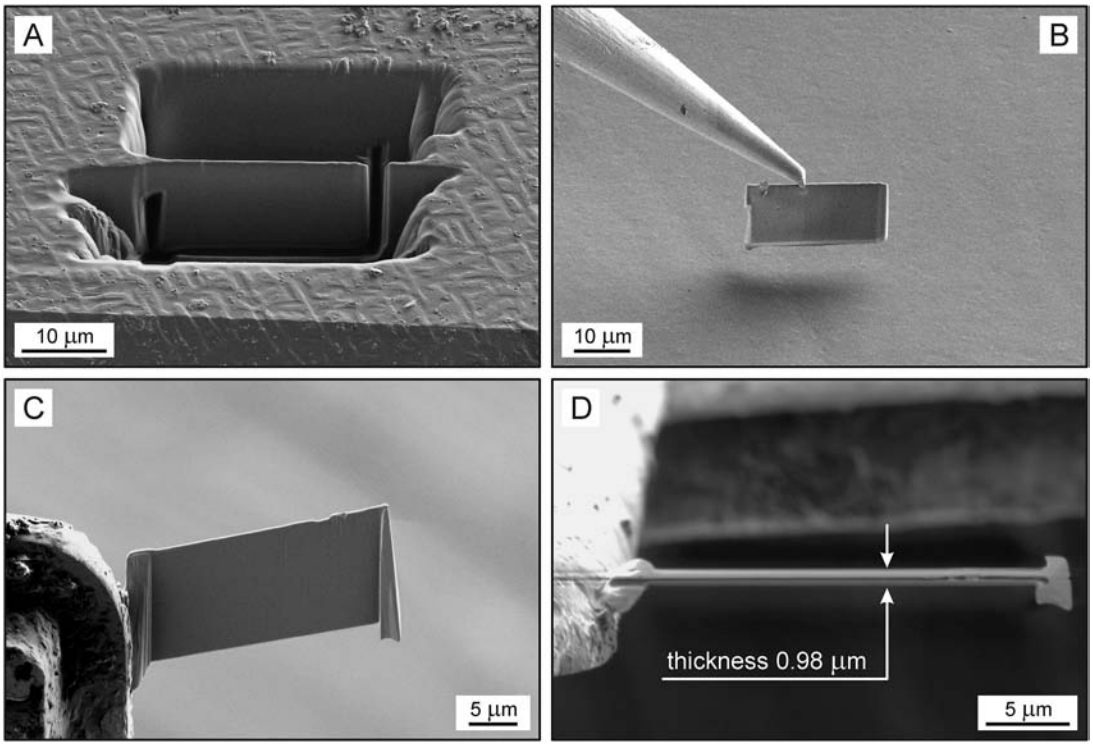

FIG. 1. Series of secondary electron (SE) images to visualize the sample-preparation procedure. (A) Prism face of a monazite-(Ce) crystal with two rectangular, ion-beam cut-holes, which bracket a narrow "wall" (*i.e.*, the future lamella to be prepared). (B) Cut-out lamella of monazite-(Ce) attached to the tip of a micro-manipulator. (C) Monazite-(Ce) lamella after final ion-beam thinning. The left edge is attached to a TEM copper grid by Pt deposition. (D) Same lamella after tilting (view along the tabular face).

linear background and assuming Lorentzian–Gaussian band shapes. The FWHM (full width at half-maximum) valences are reported as measured. Note, however, that for quantitative purposes, fitted values of FWHM need to be corrected mathematically for the experimental broadening (*i.e.*, the apparatus function of the Raman system used), as documented by Irmer (1985) and Verma *et al.* (1995).

RESULTS AND DISCUSSION

To get estimates of the extent and depth distribution of damage in the Au-irradiated monazite, Monte Carlo simulations using the SRIM program (Ziegler *et al.* 1985) were done. The SRIM (Stopping and Range of Ions in Matter) software is a collection of packages that, among other features, allows one to calculate the damage to solid targets caused by injected ions based on a full quantum-mechanical treatment of ion–atom collisions in the target. In our calculations, SRIM default values were accepted for binding energies (3 eV) and displacement energies (25 eV for Ce and P, and 28 eV for O) of target atoms, and the $CePO_4$ target density was assumed to be 5.2 g/cm^3. For sufficient statistical precision, trajectories for 1000 incoming Au ions (assumed to be irradiated perpendicular to the target surface) were calculated. Results (Fig. 2) suggest that (i) an average of ~23,600 target vacancies are generated per single incoming Au ion, and (ii) these point defects are located in a zone that extends ≤1.5 μm into the sample. The latter prediction is consistent with the TEM observations of Picot *et al.* (2008; see Fig. 6 in that study).

The above values allow us to estimate the densities of defects in the irradiated zones. The lowest fluence of 0.6×10^{13} Au ions per cm^2 corresponds to ~1.4×10^{17} generated vacancies per cm^2, which are distributed within a monazite zone 1.5 μm thick. Monazite (space group $P2_1/n$; Z = 4) contains 24 atoms per unit cell (volume ~300 Å^3; Ni *et al.* 1995); therefore, a monazite zone 1.5 μm thick consists of ~1.2×10^{19} lattice atoms per cm^2. The ratio of the above two values suggests that irradiation of monazite with 0.6×10^{13} ions/cm^2 has resulted in a damaged zone 1.5 μm thick, with an average density of defects of ~0.01 dpa (displacements

per lattice atom). Analogous calculations for the other three irradiations yield average densities of defects of ~0.04 dpa (1.8×10^{13} ions/cm^2), ~0.11 dpa (5.4×10^{13} ions/cm^2), and ~1.00 dpa (5.1×10^{14} ions/cm^2). These values are not considered to be very accurate, mainly because default values for displacement energies were used in our calculations. However, it is known that realistic values of displacement energy tend to be somewhat higher than the SRIM defaults. To give two examples, Uzan-Saguy *et al*. (1995) used a displacement energy of 45 eV to calculate defects in ion-irradiated diamond (the SRIM default for C is 28 eV), and Williford *et al*. (1998) calculated values of displacement energy of approximately 90 eV for Zr, 20 eV for Si, and 53 eV for O for $ZrSiO_4$ (SRIM defaults are 25 eV, 15 eV, and 28 eV, respectively). It thus seems reasonable to assume that the SRIM default values for displacement energy are also slightly too low for a $CePO_4$ target, which in turn would result in calculated numbers of vacancies that are slightly too high, and hence slightly too high estimates of defect density. In spite of this uncertainty, our calculations suggest that in the case of the three lower-dose irradiation experiments ($0.6–5.4 \times 10^{13}$ ions/cm^2), the surficial zone ≤1.5 μm thick has experienced low to moderate radiation-damage, whereas the highest-dose irradiation (5.1×10^{14} ions/cm^2) has resulted in an average density of damage well above the amorphization level (*e.g*., Weber *et al*. 1994).

Spectroscopic results are presented in Figure 3. Lamellae that were irradiated with $0.6–5.4 \times 10^{13}$ ions/cm^2 yield internal PO_4 vibrational Raman bands that are clearly broadened, compared to their analogs in the spectrum of the unirradiated lamella. The band broadening correlates well with the irradiation dose and is accompanied by general losses in intensity and slight shifts of bands toward lower wavenumbers. For instance, the FWHM of the main band in monazite, which is assigned to the symmetric stretching of PO_4 tetrahedra, increased from 4.6 cm^{-1} (unirradiated) to 14.6 cm^{-1} (5.4×10^{13} ions/cm^2), and its spectral position shifted from 969 cm^{-1} (unirradiated) to 965 cm^{-1} (5.4×10^{13} ions/cm^2), respectively. The detection of "crystalline" PO_4 bands in these samples suggests that the three lamellae irradiated with up to 5.4×10^{13} Au ions per cm^2 have experienced notable irradiation-induced damage but still contain a major crystalline volume-fraction, which agrees well with the SRIM results discussed above. In contrast, the spectrum of the lamella that was irradiated with the highest fluence (5.1×10^{14} ions/cm^2) no longer shows distinct PO_4 bands. Only extremely broad humps were detected, which resemble the Raman signal of fully metamict, amorphized minerals (Nasdala *et al*. 2003, Tomasic *et al*. 2004, Gieré *et al*. 2009), indicating irradiation-induced amorphization; this is again in agreement with the predicted high density of defects of ~1.00 dpa. Also, our observations seem to agree very well with results of Ar^+ (Karioris *et al*. 1982) and Kr^+ irradiation experiments (Karioris *et al*. 1981, Meldrum *et al*. 1997, 1998), in which amorphization of monazite at elevated fluences, and resulting densities of defects in the ~1 dpa range, were observed.

The spectral changes of the three lower-dose irradiated lamellae coincide very well with those of other gradually radiation-damaged minerals such as zircon (Nasdala *et al*. 1995), monazite (Seydoux-Guillaume *et al*. 2002), and cordierite (Nasdala *et al*. 2006). The band broadening, which reflects the general decrease of the lifetime of phonons, is assigned mainly to the decreasing short-range order resulting from the irradiation (accumulation of point defects and increasing irregularity of the PO_4 tetrahedra in the lattice). The accompanying slight down-shift of the band indicates moderate expansion of the P–O bonds, which in turn is assigned to both the increasing irregularity of the lattice (distortion and tilting of PO_4 tetrahedra) and dilative strain caused by the presence of (volume-expanded) amorphous clusters. In conclusion, there is no special behavior of phosphate groups in an irradiated solid, as was claimed by Picot *et al*. (2008).

A small but non-negligible fraction of the observed FWHM increase and downshift of the Raman bands, however, is an artifact resulting from the sample preparation. As expected, the spectrum of the unirradiated lamella is already slightly broadened and lower in

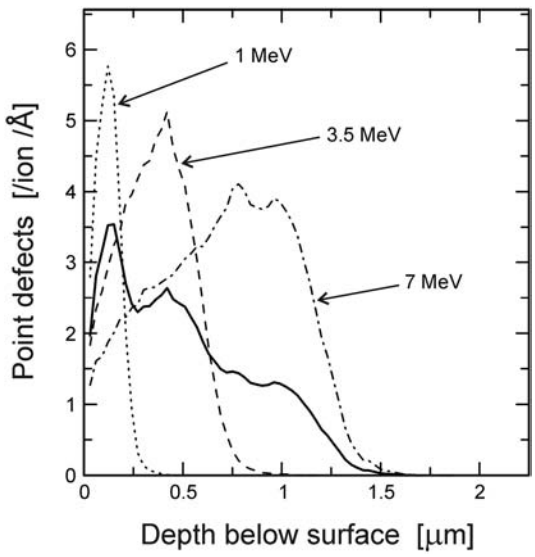

FIG. 2. Lateral distribution of point defects (*i.e*., atomic displacements minus immediate replacement collisions) generated by the irradiation with 1, 3.5, and 7 MeV Au ions in a monazite-(Ce) target, as predicted by Monte Carlo simulations (solid graph: average of the triple irradiation). The damaged zone extends ≤1.5 μm into the host crystal.

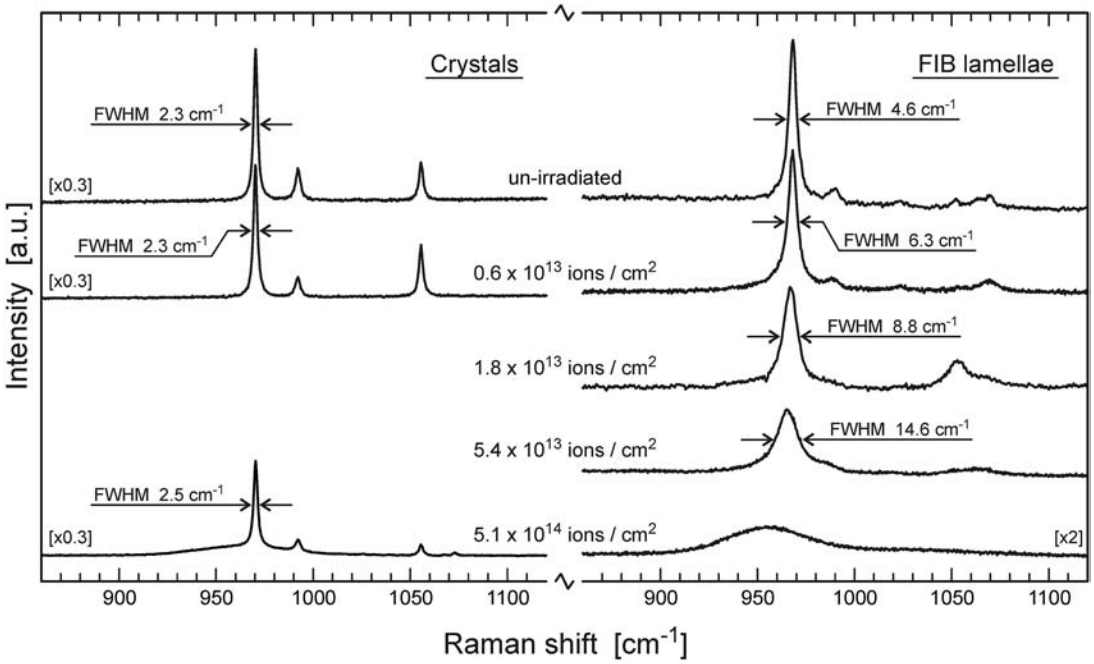

FIG. 3. Raman spectra of five lamellae of monazite (right). With increasing Au ion irradiation (total fluences are given in the center), the symmetric PO_4 stretching band at ~970 cm^{-1} broadens and shifts toward lower wavenumbers. The sample irradiated with the highest dose no longer shows any significant Raman signal of crystalline $CePO_4$. The three Raman spectra on the left side were obtained from simultaneously irradiated, unprepared crystals. These spectra are dominated by the narrow PO_4 stretching bands of the host crystals underneath the surficial volume of irradiation-damaged sample.

intensity, compared to that of the unirradiated crystal [the intense $\nu_1(PO_4)$ band in the latter lies at 970 cm^{-1} and has a FWHM of only 2.3 cm^{-1}]. These spectral differences (Fig. 3) show that the vibrational spectroscopic responses of the thin lamellae (whose thicknesses are less than two times the excitation wavelength) are not fully equivalent to that of bulk crystals, because of an increasing contribution of surface effects (Salje 1973) and perhaps also some extent of strain in the thin foils. For future experiments, it appears worthwhile, therefore, to consider alternative techniques of preparation such as thin-film deposition onto a "Raman-inert" substrate material, especially if phenomena with depths well below 1 μm are to be studied. In our case, however, the preparation-induced changes to the spectra of ~1 μm thick lamella are small, compared to the irradiation-induced changes, and hence they do not affect the validity of our observations and conclusions.

Most importantly, the significant Raman spectral changes caused by the irradiation damage are only observed from the thin lamellae, whereas the spectra of all (*i.e.*, unirradiated and irradiated) crystals are dominated by narrow PO_4 vibrations, similar to what has been described by Picot *et al.* (2008). The only indication of irradiation damage in the crystals is the appearance of the broad "amorphous" hump near 960 cm^{-1} as a weak background feature (see bottom left spectrum in Fig. 3); this feature is also evident in the spectra published by Picot *et al.* (2008). As our crystals and lamellae consist of the same material and were subjected to identical, simultaneous irradiation, and hence have experienced the same amount of damage, the different Raman spectra must be due to different sample-volumes analyzed. We conclude that in case of the crystals, the host behind the surficial irradiation-damaged zone is a major, and even dominant, contribution to the Raman spectra. According to the general estimate of $\sim 4\lambda/(NA)^2$, a theoretically possible depth-resolution of ~3.1 μm (in air) is calculated for our measurements. However, the real experimental axial resolution of a confocal spectrometer system is normally notably higher than the theoretically predicted maximum performance (Bruneel *et al.* 2002, Tfayli *et al.* 2008). Approximate assessments that consider the high refractivity of monazite (see procedures described in Everall 2000, Baldwin & Batchelder 2001) scatter well above 6 μm. It thus appears reasonable to assume that a volume extending to at least 3 μm above and

below the focal plane, or an even larger volume, was analyzed in our experiments.

The principal relation of analyzed volume and irradiation-damaged volume is visualized in Figure 4. The analyzed volume above the focal plane lies above the sample surface, *i.e.*, it consists of air and hence it does not contribute to the Raman spectrum obtained in the PO_4 stretching region. However, the Raman signal scattered from the volume in the range between 1.5 and >3 μm (?) below the sample surface (undamaged host crystal) has tremendous effects on the spectrum obtained. In addition, a confocal arrangement of the spectrometer's optical pathway does not result in full obliteration, but merely significant reduction, of light that is scattered (Raman) or emitted (luminescence) outside the range of depth resolution. Consequently, the effectively analyzed volume of sample will increase further if the phase to be analyzed is in close proximity to another phase with much higher scattering cross-section (Everall 2008, 2009), or a highly luminescent phase. This was the case in our measurements, with the radiation-damaged zone (significantly lowered scattering intensity) to be analyzed being located atop the crystalline host (higher scattering intensity).

In conclusion, even the use of a well-performing confocal Raman spectrometer did not allow us to analyze separately a ≤1.5 μm thick, radiation-damaged zone atop its underlying crystalline host. Thorough analysis was only possible through the use of ~1 μm thin lamellae. The FIB preparation of these lamellae was virtually equivalent to the mechanical pre-removal of the crystalline host behind the irradiation-damaged zone. This example demonstrates strikingly how dramatic can be the effects of a false estimation of sample volumes to be analyzed in relation to the sample volumes actually analyzed.

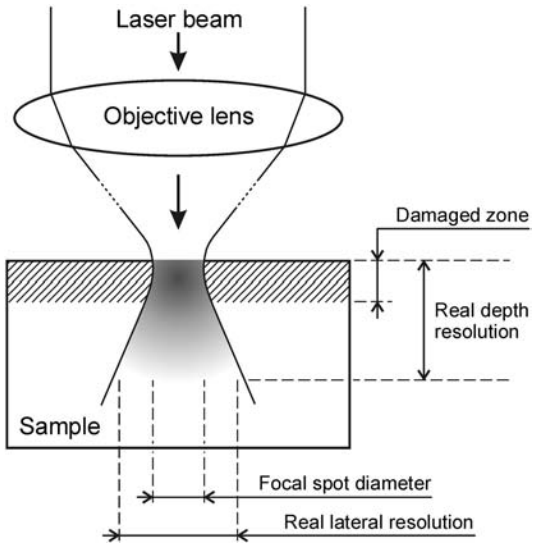

FIG. 4. Simplified sketch (not to scale) of the beam path of a confocal Raman spectrometer near the focused surface of the sample. The analyzed volume-area is shown in gray. Its extension below the sample surface exceeds appreciably the depth of the irradiation-damaged zone (hatched). Note also that the real lateral resolution exceeds the focal-spot size.

ACKNOWLEDGEMENTS

The synthetic $CePO_4$ crystals used in this study were kindly made available by K. Ruschel and J.M. Hanchar. Thanks are due to W. Hofmeister and T. Häger for the opportunity to use the confocal Raman spectrometer at the Institute for Gemstone Research, Mainz. We are most grateful to two anonymous referees and editor R.F. Martin for their constructive and helpful comments. This research was funded partially by the European Commission through contract MEXC–CT–2005–024878 and Research Infrastructures Transnational Access (RITA) contract no. 025646, and the Austrian Science Fund (FWF) through grant P20028–N10.

REFERENCES

ANDERSON, A.J., WIRTH, R. & THOMAS, R. (2008): The alteration of metamict zircon and its role in the remobilization of high-field-strength elements in the Georgeville granite, Nova Scotia. *Can. Mineral.* **46**, 1-18.

BALDWIN, K.J. & BATCHELDER, D.N. (2001): Confocal Raman microspectroscopy through a planar interface. *Appl. Spectrosc.* **55**, 517-524.

BRUNEEL, J.L., LASSÈGUES, J.C. & SOURISSEAU, C. (2002): In-depth analyses by confocal Raman microspectrometry: experimental features and modeling of the refraction effects. *J. Raman Spectrosc.* **33**, 815-828.

DELATTRE, S., UTSUNOMIYA, S., EWING, R.C., BOEGLIN, J.-L., BRAUN, J.-J., BALAN, E. & CALAS, G. (2007): Dissolution of radiation-damaged zircon in lateritic soils. *Am. Mineral.* **92**, 1978-1989.

DIAS, A.N.C., SAENZ, C.A.T., CONSTANTINO, C.J.L., SOARES, C.J., NOVAES, F.P. & BALAN, A.M.O.A. (2009): Micro-Raman spectroscopy and SEM/EDX applied to improve the zircon fission track method used for dating geological formations. *J. Raman Spectrosc.* **40**, 101-106.

EVERALL, N.J. (2000): Modelling and measuring the effect of refraction on the depth resolution of confocal Raman microscopy. *Appl. Spectrosc.* **54**, 773-782.

EVERALL, N.J. (2008): The influence of out-of-focus sample regions on the surface specifity of confocal Raman microscopy. *Appl. Spectrosc.* **62**, 591-598.

EVERALL, N.J. (2009): Confocal Raman microscopy: performance, pitfalls, and best practice. *Appl. Spectrosc.* **63**, 245A-262A.

EVERALL, N.J., LAPHAM, J., ADAR, F., WHITLEY, A., LEE, E. & MAMEDOV, S. (2007): Optimizing depth resolution in confocal Raman microscopy: a comparison of metallurgical, dry corrected, and oil immersion objectives. *Appl. Spectrosc.* **61**, 251-259.

EWING, R.C. & WANG, LUMIN (2002): Phosphates as nuclear waste forms. *In* Phosphates: Geochemical, Geobiological, and Materials Importance (M.J. Kohn, J. Rakovan & J.M. Hughes, eds.). *Rev. Mineral. Geochem.* **48**, 673-699.

GIERÉ, R., WILLIAMS, C.T., WIRTH, R. & RUSCHEL, K. (2009): Metamict fergusonite-(Y) in a spessartine-bearing granitic pegmatite from Adamello, Italy. *Chem. Geol.* **261**, 333-345.

HANCHAR, J.M., FINCH, R.J., HOSKIN, P.W.O., WATSON, E.B., CHERNIAK, D.J. & MARIANO, A.N. (2001): Rare earth elements in synthetic zircon. 1. Synthesis, and rare earth element and phosphorus doping. *Am. Mineral.* **86**, 667-680.

HAYAZAWA, N., MOTOHASHI, M., SAITO, Y., ISHITOBI, H., ONO, A., ICHIMURA, T., VERMA, P. & KAWATA, S. (2007): Visualization of localized strain of a crystalline thin layer at the nanoscale by tip-enhanced Raman spectroscopy and microscopy. *J. Raman Spectrosc.* **38**, 684-696.

IRMER, G. (1985): Zum Einfluß der Apparatefunktion auf die Bestimmung von Streuquerschnitten und Lebensdauern aus optischen Phononenspektren. *Exper. Techn. Phys.* **33**, 501-506.

KARIORIS, F.G., APPAJI GOWDA, K. & CARTZ, L. (1981): Heavy-ion bombardment of monoclinic $ThSiO_4$, ThO_2 and monazite. *Radiat. Eff. Lett.* **58**, 1-3.

KARIORIS, F.G., APPAJI GOWDA, K., CARTZ, L. & LABBE, J.C. (1982): Damage cross-sections of heavy ions in crystal structures. *J. Nucl. Mater.* **108–109**, 748-750.

KEEN, I., RINTOUL, L. & FREDERICKS, P.M. (2002): Raman microspectroscopic mapping: a tool for the characterisation of polymer surfaces. *Macromol. Symp.* **184**, 287-298.

MELDRUM, A., BOATNER, L.A. & EWING, R.C. (1997): Displacive radiation effects in the monazite- and zircon-structure orthophosphates. *Phys. Rev. B* **56**, 13805-13814.

MELDRUM, A., BOATNER, L.A., WEBER, W.J. & EWING, R.C. (1998): Radiation damage in zircon and monazite. *Geochim. Cosmochim. Acta* **62**, 2509-2520.

NASDALA, L. (2009): Pb^+ irradiation of synthetic zircon ($ZrSiO_4$): infrared spectroscopic investigation – discussion. *Am. Mineral.* **94**, 853-855.

NASDALA, L., IRMER, G. & WOLF, D. (1995): The degree of metamictization in zircon: a Raman spectroscopic study. *Eur. J. Mineral.* **7**, 471-478.

NASDALA, L., KRONZ, A., GRAMBOLE, D. & TRULLENQUE, G. (2007): Effects of irradiation damage on the back-scattering of electrons: silicon-implanted silicon. *Am. Mineral.* **92**, 1768-1771.

NASDALA, L., SMITH, D.C., KAINDL, R. & ZIEMANN, M. (2004): Raman spectroscopy: analytical perspectives in mineralogical research. *In* Spectroscopic Methods in Mineralogy (A. Beran & E. Libowitzky, eds.). *Eur. Mineral. Union Notes in Mineralogy* **6**, 281-343.

NASDALA, L., WILDNER, M., WIRTH, R., GROSCHOPF, N., PAL, D.C. & MÖLLER, A. (2006): Alpha particle haloes in chlorite and cordierite. *Mineral. Petrol.* **86**, 1-27.

NASDALA, L., ZHANG, MING, KEMPE, U., PANCZER, G., GAFT, M., ANDRUT, M. & PLÖTZE, M. (2003): Spectroscopic methods applied to zircon. *In* Zircon (J.M. Hanchar & P.W.O. Hoskin, eds.). *Rev. Mineral. Geochem.* **53**, 427-467.

NI, YUNXIANG, HUGHES, J.M. & MARIANO, A.N. (1995): Crystal chemistry of the monazite and xenotime structures. *Am. Mineral.* **80**, 21-26.

PICOT, V., DESCHANELS, X., PEUGET, S., GLORIEUX, B., SEYDOUX-GUILLAUME, A.M. & WIRTH, R. (2008): Ion beam radiation effects in monazite. *J. Nucl. Mater.* **381**, 290-296.

RAINERI, V., GALVAGNO, G., RIMINI, E., BIERSACK, J.P., NAKAGAWA, S.T., LA FERLA, A. & CARNERA, A. (1991) Channelling implants of B ions into silicon surfaces. *Radiat. Eff. Defects in Solids* **116**, 211-217.

SALJE, E. (1973): Experimentelle Untersuchung der Ramanstreuung an Kristallpulvern. *J. Appl. Crystallogr.* **6**, 442-446.

SEYDOUX-GUILLAUME, A.-M., WIRTH, R., NASDALA, L., GOTTSCHALK, M., MONTEL, J.M. & HEINRICH, W. (2002): An XRD, TEM and Raman study of experimentally annealed natural monazite. *Phys. Chem. Minerals* **29**, 240-253.

TABAKSBLAT, R., MEIER, R.J. & KIP, B.J. (1992): Confocal Raman microspectroscopy: theory and application to thin polymer samples. *Appl. Spectrosc.* **46**, 60-68.

TFAYLI, A., PIOT, O. & MANFAIT, M. (2008): Confocal Raman microspectroscopy on excised human skin: uncertainties in depth profiling and mathematical correction applied to dermatological drug permeation. *J. Biophoton.* **1**, 140-153.

TOMAŠIC, N., GAJOVIĆ, A., BERMANEC, V. & RAJIĆ, M. (2004): Recrystallization of metamict Nb–Ta–Ti–REE complex oxides: a coupled X-ray-diffraction and Raman spectroscopy study of aeschynite-(Y) and polycrase-(Y). *Can. Mineral.* **42**, 1847-1857.

UZAN-SAGUY, C., CYTERMANN, C., BRENER, R., RICHTER, V., SHAANAN, M. & KALISH, R. (1995): Damage threshold for ion-beam induced graphitization of diamond. *Appl. Phys. Lett.* **67**, 1194-1196.

VERMA, P., ABBI, S.C. & JAIN, K.P. (1995): Raman-scattering probe of anharmonic effects in GaAs. *Phys. Rev. B* **51**, 16660-16667.

WEBER, W.J., EWING, R.C. & WANG, L.-M. (1994): The radiation-induced crystalline-to-amorphous transition in zircon. *J. Mater. Res.* **9**, 688-698.

WILLIAMS, K.P.J., PITT, G.D., BATCHELDER, D.N. & KIP, B.J. (1994): Confocal Raman microspectroscopy using a stigmatic spectrograph and CCD detector. *Appl. Spectrosc.* 48, 232-235.

WILLIFORD, R.E., DEVANATHAN, R. & WEBER, W.J. (1998): Computer simulation of displacement energies for several ceramic materials. *Nucl. Instrum. Meth. B* **141**, 94-98.

WILSON, T. (1989): Trends in confocal microscopy. *Trends Neurosci.* **12**, 486-493.

WIRTH, R. (2004): Focused Ion Beam (FIB): a novel technology for advanced application of micro- and nanoanalysis in geosciences and applied mineralogy. *Eur. J. Mineral.* **16**, 863-876.

ZHANG, MING, BOATNER, L.A., SALJE, E.K.H., EWING, R.C., DANIEL, P., WEBER, W.J., ZHANG, YANWEN & FARNAN, I. (2008): Micro-Raman and micro-infrared spectroscopic studies of Pb- and Au-irradiated $ZrSiO_4$: optical properties, structural damage, and amorphization. *Phys. Rev. B* **77**, 144110.

ZIEGLER, J.F., BIERSACK, J.P. & LITTMARK, U. (1985): *The Stopping and Range of Ions in Solids*. Pergamon Press, New York, N.Y.

Received October 2, 2009, revised manuscript accepted March 2, 2010.